High-brightness tapered quantum cascade lasers

Cite as: Appl. Phys. Lett. **102**, 053503 (2013); https://doi.org/10.1063/1.4791557
Submitted: 28 November 2012 . Accepted: 28 January 2013 . Published Online: 05 February 2013

Burç Gökden, Tobias S. Mansuripur, Romain Blanchard, Christine Wang, Anish Goyal, Antonio Sanchez-Rubio, George Turner, and Federico Capasso

High-brightness tapered quantum cascade lasers

Burç Gökden,[1] Tobias S. Mansuripur,[2] Romain Blanchard,[1] Christine Wang,[3] Anish Goyal,[3] Antonio Sanchez-Rubio,[3] George Turner,[3] and Federico Capasso[1,a)]
[1]*Harvard University School of Engineering and Applied Sciences, 29 Oxford St., Cambridge, Massachusetts 02138, USA*
[2]*Harvard University Department of Physics, 17 Oxford St., Cambridge, Massachusetts 02138, USA*
[3]*MIT Lincoln Laboratory, 244 Wood St., Lexington, Massachusetts 02420, USA*

(Received 28 November 2012; accepted 28 January 2013; published online 5 February 2013)

An index-guided tapered quantum cascade laser emitting near 9.5 μm with sloped sidewalls and no anti-reflection coating is presented, and the performance for devices with taper half-angles of 1° and 2° is investigated. The 1° device delivers up to 2.5 W of peak optical power at room temperature with beam quality-factor $M^2 = 2.08$, while the two-degree device outputs 3.8 W with $M^2 = 2.25$ for a maximum brightness of 1.87 MW cm^{-2} sr^{-1}. © *2013 American Institute of Physics*. [http://dx.doi.org/10.1063/1.4791557]

Quantum cascade lasers (QCLs) are prominent sources of mid-infrared (mid-IR) radiation due to their compact size and high performance. Wavelength agility is achieved by tailoring the intersubband transition to a specific wavelength using bandstructure engineering.[1] With recent improvements in material quality and device performance,[2,3] QCLs are becoming the coherent light source of choice for applications in the mid-IR spectrum, such as gas sensing[4] and infrared countermeasures. For these applications, high-power output, narrow beam width, and high wall-plug efficiency are desirable features. While high-power QCLs can be obtained by increasing the device area, their beam profile degrades quickly as higher-order lateral cavity modes are excited. To account for this tradeoff between beam quality and power, it is important to maximize the brightness of the laser given by $B = P/(\lambda^2 M_x^2 M_y^2)$, where P is the total emitted power, λ is the wavelength, and $M_{x,y}^2 = (4\pi/\lambda)\sigma_{0x,y}\sigma_{\theta x,y}$, where σ_0 and σ_θ are the standard deviations of the near-field spatial intensity profile and the far-field angular intensity profile, respectively, in either the x or y directions.[5,6] The M^2 value is the ratio of the divergence angle of the laser to the divergence angle of a Gaussian beam whose waist is equal to the waist of the laser beam $w \equiv 2\sigma_0$, so that $M_{x,y}^2 = 1$ for a diffraction-limited beam and larger otherwise. For semiconductor lasers, we can take $M_y^2 = 1$, due to the strong vertical mode confinement, and consider only the beam distortion in the lateral direction.

One method of achieving high brightness is the master oscillator/tapered amplifier (MOPA) geometry, in which the output of a nearly diffraction-limited seed laser is directed through a tapered gain section, which acts as a traveling-wave amplifier. The broader area of the tapered section mitigates the effect of gain saturation on reducing the single-pass gain. Such an architecture has been implemented in both interband lasers using gain guiding[7] and QCLs using index guiding.[8,9] To prevent lasing in the amplifier section, the front facet can be antireflection (AR) coated[7,9] or cleaved at a small angle relative to the normal to the propagating direction.[8] Since QCLs can be tailored to emit across a broad range of the mid-IR spectrum, the design of an AR coating for broadband MOPA QCLs becomes a very challenging issue. The need for an AR coating at the facet also makes the fabrication of integrated photonic circuits coupled to a MOPA QCL difficult. Furthermore, the MOPA devices require separate electrical contacts for the seed and amplifier sections.

Tapered lasers are a different approach in which the laser oscillation takes place in the combined tapered and seed sections and require only a single top contact. A short ridge waveguide section is followed by a tapered waveguide section, which expands at an angle smaller than the free diffraction angle of the fundamental mode of the ridge. (Such a geometry is also useful for improving the outcoupling of terahertz radiation generated by difference frequency generation in QCLs.[10,11]) The ridge is narrow enough that the losses for higher-order lateral modes are substantially greater than for the fundamental mode; the preferred fundamental mode is then adiabatically expanded in the tapered section. Such tapered QCLs have been demonstrated with vertical sidewalls, an AR coating on the wide facet and high-reflectivity coating on the narrow facet, but the peak output power was limited to 200 mW.[12] To further improve the beam quality, we propose to enhance the loss disparity between the fundamental and higher-order lateral modes in the ridge section using curved sidewalls, which were recently shown to introduce additional losses in the form of reflection into the InP bulk as well as plasmonic losses.[13] Although this loss is detrimental for a narrow Fabry-Pérot (FP) ridge laser because it affects the fundamental mode as well, the additional losses are even greater for the higher-order modes, which have greater intensity near the walls. In this Letter, we characterize the beam quality and output power for two different tapered QCL waveguide designs with curved sidewalls and no AR coatings.

The material used in this study was based on a bound-to-continuum active region design optimized for high-power, high-temperature operation with a relatively broad gain spectrum.[14] The QCL active region was grown on an InP wafer by metal-organic chemical vapor deposition (MOCVD), and comprised 35 repetitions of the superlattice structure given

a)capasso@seas.harvard.edu.

by **4.4**/1.7/**0.9**/5.3/**1.1**/5.2/**1.2**/4.7/**1.3**/4.2/**1.5**/3.9/**1.6**/3.4/**1.8**/3.1/**2.1**/2.8/**2.5**/2.7/**3.2**/2.7/**3.6**/2.5, where thicknesses are given in nanometers for InAlAs barriers (boldface) and InGaAs wells. The underlined section was n-doped by silicon with a doping density of 1.5e17 cm^{-3}. The 2.3-μm-thick active region was sandwiched between two 0.5-μm-thick InGaAs spacer layers followed by a 3.5-μm-thick InP cladding and a 520-nm-thick highly doped InP cap layer. The growth ends with a highly doped 20-nm-thick InGaAs contact layer.

The top view of the tapered laser cavity geometry is shown schematically in Fig. 1(a). The ridge section was 0.5-mm-long with an average active region width of 14 μm; the tapered section was 2.5-mm-long and characterized by the taper half-angle θ, which was either 0° (i.e., standard FP ridge), 1°, or 2°. The wafer was wet etched down to 9.5 μm (just beyond the active region) resulting in sidewalls inclined at about 37° to the horizontal. Scanning electron microscope (SEM) images of the back and front laser facets are shown in Figs. 1(b) and 1(c) for the 2° device. The device was passivated by depositing a 500-nm-thick silicon nitride layer on the ridge, and a single top contact window was opened in the nitride by inductively coupled plasma etching. After a Ti/Au metal deposition for the top contact, the sample was thinned down to 200 μm and Ti/Au was deposited as the bottom contact. An additional 4 μm of gold was deposited on the top contact by electroplating for improved heat dissipation. The devices were then cleaved and indium-soldered epi-side-up on a copper heat sink. The laser facets were left uncoated. For all measurements, the lasers were driven in pulsed operation (100-ns pulse width and 0.2% duty-cycle) at 20 °C on a Peltier cooler.

Figure 2 shows the L-I and I-V characteristics of 0°, 1°, and 2° tapered QCLs, where the output power is measured from the front facet only. In order of increasing taper angle, the maximum peak output power was 0.84, 2.55, and

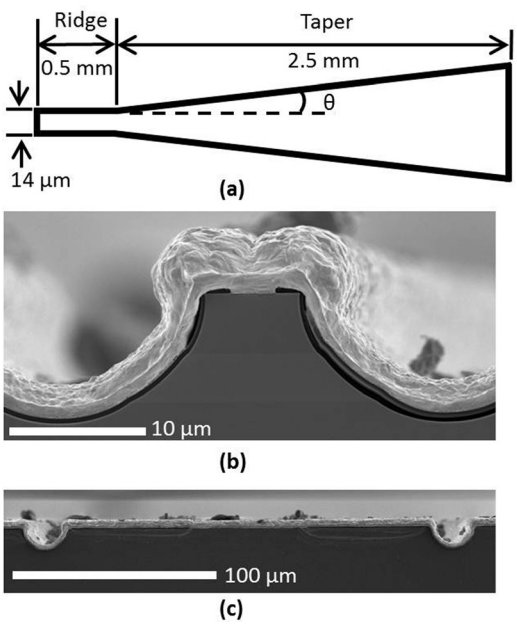

FIG. 1. (a) Schematic of top view of the tapered laser waveguide, as well as representative SEM images of (b) the back facet and (c) the front facet of the 2° device.

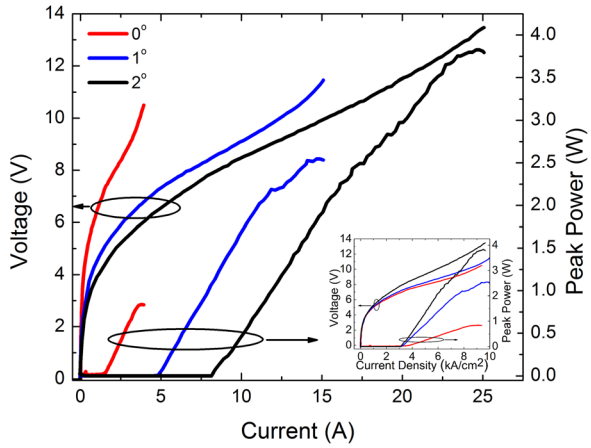

FIG. 2. The L-I and I-V curves shown for the three devices with taper half-angles 0°, 1°, and 2°. The optical power is measured from the front facet of each device. Inset: same curves plotted on a current density scale.

3.83 W, the slope efficiency was 403, 315, and 300 mW/A, and the threshold current density was $J_{th} = 3.44$, 3.14, and 3.16 kA/cm^2 (see inset of Fig. 2). Strictly speaking, the usual expressions for threshold current and slope efficiency of a semiconductor laser—which are based on the assumptions of constant waveguide width and a photon density that is independent of position along the propagation direction—cannot be applied to tapered lasers, and deriving appropriate expressions for tapered lasers is beyond the scope of this work. Nevertheless, we can draw some general conclusions about the laser characteristics from the data. The reduction in slope efficiency with increasing taper angle can be ascribed to higher optical losses due to any non-adiabaticity of the taper. (It is also reasonable to expect that large-area devices have poorer heat dissipation, resulting in additional losses due to intra-pulse heating. We have experimentally confirmed that this effect is significant even for pulse widths as short as 50 ns, but only for currents greater than about 70% of the rollover current. The slope efficiency is determined by a linear fit to the L-I curve at lower currents, and is therefore not affected by intra-pulse heating.) We can roughly quantify the waveguide loss α_w of the FP device from its slope efficiency by assuming an internal differential quantum efficiency[15] of 0.79,[14] as well as a facet power reflectivity of 0.27 (corresponding to a mirror loss $\alpha_m = 4.34\ cm^{-1}$), which results in $\alpha_w = 15.1\ cm^{-1}$. Although the slope efficiency decreases with increasing taper angle, paradoxically, the threshold current density is also lower for the tapered devices than for the FP device. This can be explained, however, if the modal gain (a quantity which affects the threshold but not the slope efficiency) is larger for tapered lasers, which is reasonable to expect based on the larger confinement factor of wider devices.

Lasing spectra of the 2° device were measured using a Fourier-transform infrared (FTIR) spectrometer at a resolution of 0.1 cm^{-1} for different current levels as shown in Fig. 3. The spectrum spans a wavelength range of more than 500 nm, centered at 9.45 μm. The mode spacing for tapered lasers and FP lasers is similar (≈4.5 nm) indicating that the effective mode index is not significantly affected by the tapered section. The spectrum shows two main groups of lasing peaks whose separation increases with the current. This

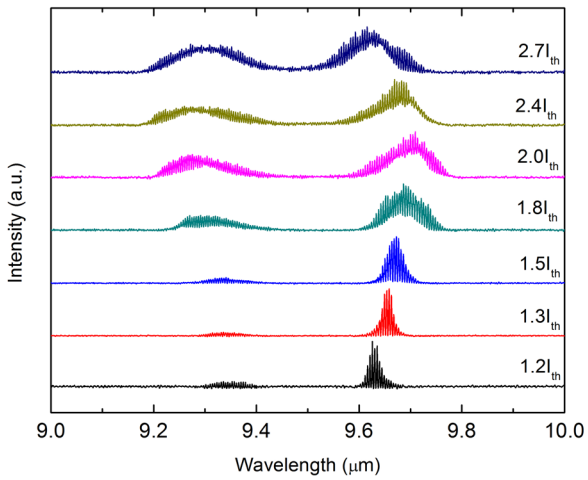

FIG. 3. The measured spectrum of the 2° device at different current levels.

spectral behavior was also observed for FP lasers with a similar active region design in Ref. 14 and has been explained in terms of Rabi oscillations of the electron population.[16]

The far-field angular intensity profiles in the lateral direction were measured with a lock-in technique using a liquid nitrogen-cooled mercury-cadmium-telluride detector placed 18 cm from the laser facet and mounted to a computer-controlled rotation stage. The far-field of the FP laser (not shown) was Gaussian with a full-width at half-maximum of 43.7° and independent of current throughout the entire operating range. The far-fields are shown for the 1° and 2° tapered QCLs at various driving currents in Figs. 4(a) and 4(b). To quantitatively analyze the beam quality, the M^2 and brightness values are plotted in Fig. 4. (For the standard deviation of the near-field intensity profile, we take the standard deviation of the fundamental mode of a slab of semiconductor with width equal to the facet width w_f ($= 101\ \mu$m for 1° and 189 μm for 2°) surrounded by a perfect electrical conductor, which gives $\sigma_0 = 0.181 w_f$.) Just above threshold ($I = 1.1\ I_{th}$), the far-field of the 1° device is Gaussian with M^2 equal to 1.48. As the current is increased, a second lobe in the far-field becomes more prominent, which results in M^2 equal to 2.08 at roll-over (equal to 3 I_{th}). This degradation of the far-field with current reduces the brightness, which reaches a maximum of 1.40 MW cm^{-2} sr^{-1} at 2.5 I_{th}. The far-field of the 2° device is also Gaussian just above threshold with M^2 equal to 2.01. It is possible that the near-field of the 2° device is narrower than the assumed waveguide mode; this would lead to a smaller M^2 value, and near-field measurements are needed to confirm this. The far-field of the 2° device broadens only slightly as the current is increased, reaching an M^2 of 2.25 at roll-over (also equal to $3I_{th}$), and a maximum brightness of 1.87 MW cm^{-2} sr^{-1}.

Asymmetric far-field profiles can result either from facet defects or the coherent superposition of multiple lateral modes.[17] As seen in Fig. 1(c), the front facets of the 1° and 2° devices are not defect-free, which is likely due to strain between the thick gold, silicon nitride, and InP top cladding, which affects the cleaving process. In future devices, this problem can be mitigated by not electroplating thick gold in the region to be cleaved, and the cause of the asymmetric far-fields can then be better elucidated.

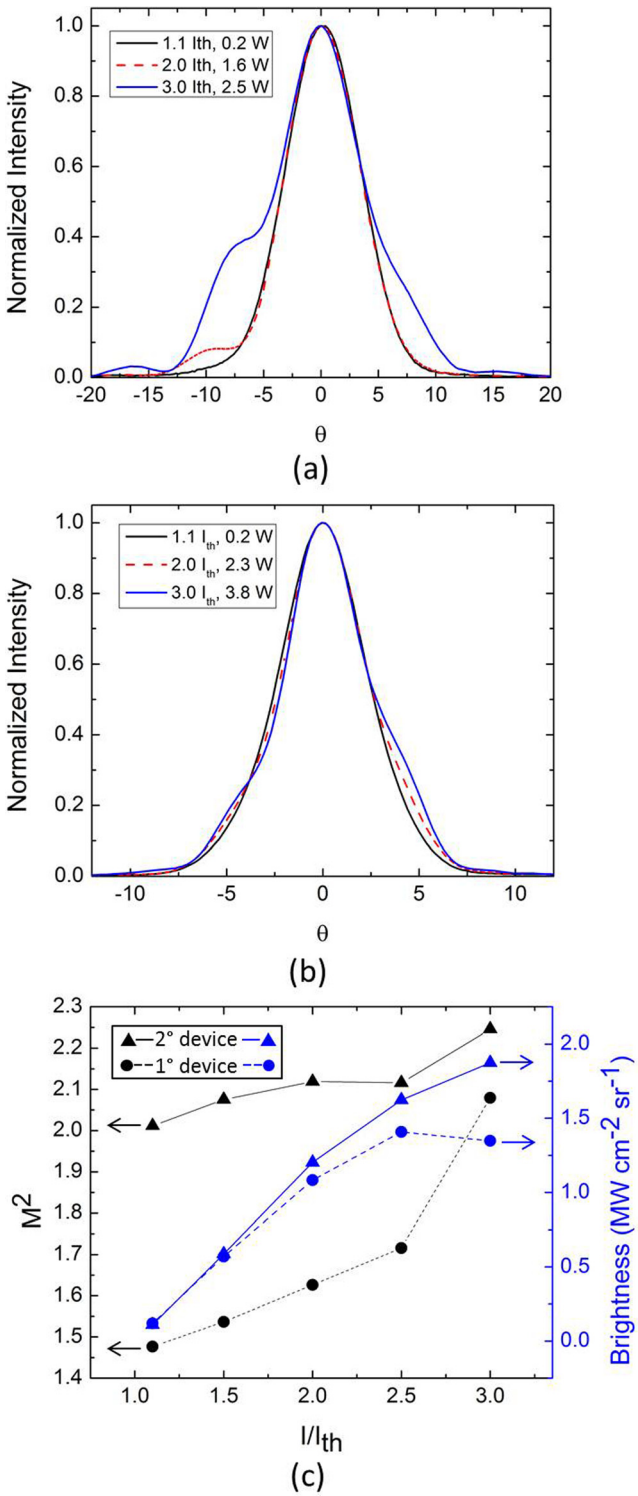

FIG. 4. The evolution of the angular far-field profiles for increasing pumping current, indicated as a multiple of the threshold current as well as the total optical output power, is shown for the (a) 1° and (b) 2° taper angles. (c) The calculated lateral M^2 beam quality factors (black) and brightness values (blue) for the 1° (dashed, circles) and 2° (solid, triangles) devices.

To determine the reproducibility of the results, the far-fields of two additional devices for each taper angle were measured, and the side-lobe of the 1° device is consistently larger than that of the 2° device, although its magnitude relative to the central peak at $\theta = 0$ varies. Interestingly, the L-I curves of the two additional 1° devices (not shown) exhibit a kink at about 85% of the maximum current at which the

slope efficiency suddenly increases. Above this current, we observe a peculiar behavior: the pulse-to-pulse output of the laser is not consistent. It appears that small fluctuations in initial conditions could affect which transverse mode lases from one electrical pulse to the next. This instability is not observed in any of the 2° devices and must be investigated in future work to better understand the observed far-fields.

In conclusion, high-power room-temperature operation of index-guided 1° and 2° tapered QCL lasers with sloped side-walls was demonstrated. For applications which require high power and good beam quality but do not require a single longitudinal mode, these lasers are superior to MOPAs because they require only a single top contact and no AR coating on the output facet. A peak-power level of 3.8 W was obtained for a 2° tapered device emitting around 9.5 μm, and the Gaussian far-field at threshold became only slightly distorted as the current was increased to roll-over, with M^2 increasing from 2.01 to 2.25, resulting in a maximum brightness of 1.87 MW cm^{-2} sr^{-1}. The 1° device far-field exhibited a larger distortion at the roll-over current. Future work will focus on further maximizing the brightness by varying the taper angle and the lengths of the ridge and tapered waveguide sections. The development of such easily implementable high performance lasers is a significant step towards compact, truly integrated photonic devices powered by QCLs.

We acknowledge financial support from the Defense Threat Reduction Agency under contract HDTRA1-10-1-0031. TSM is supported by an NSF Graduate Student Fellowship. Part of the device processing was done at the Center for Nanoscale Systems (CNS) at Harvard University. Harvard-CNS is a member of the National Nanotechnology Infrastructure Network (NNIN). The Lincoln Laboratory portion of this work was sponsored by the Office of the Assistant Secretary of Defense for Research and Engineering under Air Force Contract No. FA8721-05-C-0002. The opinions, interpretations, conclusions, and recommendations are those of the authors and are not necessarily endorsed by the United States Government.

[1]F. Capasso, R. Paiella, R. Martini, R. Colombelli, C. Gmachl, T. L. Myers, M. S. Taubman, R. M. Williams, C. G. Bethea, K. Unterrainer, H. Y. Hwang, D. L. Sivco, A. Y. Cho, A. M. Sergent, H. C. Liu, and E. A. Whittaker, IEEE J. Quantum Electron. **38**, 511 (2002).
[2]A. Lyakh, R. Maulini, A. Tsekoun, R. Go, S. Vonder Porten, C. Pflügl, L. Diehl, F. Capasso, and K. Patel, Proc. Natl. Acad. Sci. U.S.A. **107**, 18799 (2010).
[3]M. Razeghi, S. Slivken, Y. Bai, B. Gökden, and S. R. Darvish, New J. Phys. **11**, 125017 (2009).
[4]R. F. Curl, F. Capasso, C. Gmachl, A. A. Kosterev, B. McManus, R. Lewicki, M. Pusharsky, G. Wysocki, and F. K. Tittel, Chem. Phys. Lett. **487**, 1 (2010).
[5]G. Hatakoshi, Opt. Rev. **10**, 307 (2003).
[6]D. Bisping, D. Pucicki, M. Fischer, J. Koeth, C. Zimmermann, P. Weinmann, S. Hofling, M. Kamp, and A. Forchel, IEEE J. Sel. Top. Quantum Electron. **15**(3), 968 (2009).
[7]J. N. Walpole, E. S. Kintzer, S. R. Chinn, C. A. Wang, and L. J. Missaggia, Appl. Phys. Lett. **61**(7), 740 (1992).
[8]M. Troccoli, C. Gmachl, F. Capasso, D. L. Sivco, and A. Y. Cho, Appl. Phys. Lett. **80**, 4103 (2002).
[9]S. Menzel, L. Diehl, C. Pflügl, A. Goyal, C. Wang, A. Sanchez, G. Turner, and F. Capasso, Opt. Exp. **19**, 16229 (2011).
[10]M. A. Belkin, F. Capasso, F. Xie, A. Belyanin, M. Fischer, A. Wittmann, and J. Faist, Appl. Phys. Lett. **92**, 201101 (2008).
[11]Q. Y. Lu, N. Bandyopadhyay, S. Slivken, Y. Bai, and M. Razeghi, Appl. Phys. Lett. **99**, 131106 (2011).
[12]L. Nahle, J. Semmel, W. Kaiser, S. Hofling, and A. Forchel, Appl. Phys. Lett. **91**, 181122 (2007).
[13]X. Huang, Y. Chiu, W. O. Charles, and C. Gmachl, Opt. Express **20**, 2539 (2012).
[14]A. Wittman, T. Gresch, E. Gini, L. Hvozdara, N. Hoyler, M. Giovannini, and J. Faist, IEEE J. Quantum Electron. **44**(1), 36 (2008).
[15]K. Sang-Bae, H. Yong-Su, and D. Man-Hee, IEEE Electron. Lett. **29**, 1791 (1993).
[16]C. Y. Wang, L. Diehl, A. Gordon, C. Jirauschek, F. X. Kartner, A. Belyanin, D. Bour, S. Corzine, G. Hofler, M. Troccoli, J. Faist, and F. Capasso, Phys. Rev. A **75**, 031802(R) (2007).
[17]A. K. Wójcik, N. Yu, L. Diehl, F. Capasso, and A. Belyanin, Phys. Rev. Lett. **106**, 133902 (2011).